

Precise Measurements of Branching Fractions for D_s^+ Meson Decays to Two Pseudoscalar Mesons

M. Ablikim¹, M. N. Achasov^{10,d}, P. Adlarson⁶⁴, S. Ahmed¹⁵, M. Albrecht⁴,
A. Amoroso^{63A,63C}, Q. An^{60,48}, Anita²¹, Y. Bai⁴⁷, O. Bakina²⁹, R. Baldini Ferrolì^{23A},
I. Balossino^{24A}, Y. Ban^{38,l}, K. Begzsuren²⁶, J. V. Bennett⁵, N. Berger²⁸, M. Bertani^{23A},
D. Bettoni^{24A}, F. Bianchi^{63A,63C}, J. Biernat⁶⁴, J. Bloms⁵⁷, A. Bortone^{63A,63C}, I. Boyko²⁹,
R. A. Briere⁵, H. Cai⁶⁵, X. Cai^{1,48}, A. Calcaterra^{23A}, G. F. Cao^{1,52}, N. Cao^{1,52}, S. A. Cetin^{51B},
J. F. Chang^{1,48}, W. L. Chang^{1,52}, G. Chelkov^{29,b,c}, D. Y. Chen⁶, G. Chen¹, H. S. Chen^{1,52},
M. L. Chen^{1,48}, S. J. Chen³⁶, X. R. Chen²⁵, Y. B. Chen^{1,48}, W. Cheng^{63C}, G. Cibinetto^{24A},
F. Cossio^{63C}, X. F. Cui³⁷, H. L. Dai^{1,48}, J. P. Dai^{42,h}, X. C. Dai^{1,52}, A. Dbeyssi¹⁵, R. B. de
Boer⁴, D. Dedovich²⁹, Z. Y. Deng¹, A. Denig²⁸, I. Denysenko²⁹, M. Destefanis^{63A,63C},
F. De Mori^{63A,63C}, Y. Ding³⁴, C. Dong³⁷, J. Dong^{1,48}, L. Y. Dong^{1,52}, M. Y. Dong^{1,48,52},
S. X. Du⁶⁸, J. Fang^{1,48}, S. S. Fang^{1,52}, Y. Fang¹, R. Farinelli^{24A,24B}, L. Fava^{63B,63C},
F. Feldbauer⁴, G. Felici^{23A}, C. Q. Feng^{60,48}, M. Fritsch⁴, C. D. Fu¹, Y. Fu¹, X. L. Gao^{60,48},
Y. Gao⁶¹, Y. Gao^{38,l}, Y. G. Gao⁶, I. Garzia^{24A,24B}, E. M. Gersabeck⁵⁵, A. Gilman⁵⁶,
K. Goetzen¹¹, L. Gong³⁷, W. X. Gong^{1,48}, W. Gradl²⁸, M. Greco^{63A,63C}, L. M. Gu³⁶,
M. H. Gu^{1,48}, S. Gu², Y. T. Gu¹³, C. Y. Guan^{1,52}, A. Q. Guo²², L. B. Guo³⁵, R. P. Guo⁴⁰,
Y. P. Guo²⁸, Y. P. Guo^{9,i}, A. Guskov²⁹, S. Han⁶⁵, T. T. Han⁴¹, T. Z. Han^{9,i}, X. Q. Hao¹⁶,
F. A. Harris⁵³, K. L. He^{1,52}, F. H. Heinsius⁴, T. Held⁴, Y. K. Heng^{1,48,52}, M. Himmelreich^{11,g},
T. Holtmann⁴, Y. R. Hou⁵², Z. L. Hou¹, H. M. Hu^{1,52}, J. F. Hu^{42,h}, T. Hu^{1,48,52}, Y. Hu¹,
G. S. Huang^{60,48}, L. Q. Huang⁶¹, X. T. Huang⁴¹, Z. Huang^{38,l}, N. Huesken⁵⁷, T. Hussain⁶²,
W. Ikegami Andersson⁶⁴, W. Imoehl²², M. Irshad^{60,48}, S. Jaeger⁴, S. Janchiv^{26,k}, Q. Ji¹,
Q. P. Ji¹⁶, X. B. Ji^{1,52}, X. L. Ji^{1,48}, H. B. Jiang⁴¹, X. S. Jiang^{1,48,52}, X. Y. Jiang³⁷,
J. B. Jiao⁴¹, Z. Jiao¹⁸, S. Jin³⁶, Y. Jin⁵⁴, T. Johansson⁶⁴, N. Kalantar-Nayestanaki³¹,
X. S. Kang³⁴, R. Kappert³¹, M. Kavatsyuk³¹, B. C. Ke^{43,1}, I. K. Keshk⁴, A. Khoukaz⁵⁷, P.
Kiese²⁸, R. Kiuchi¹, R. Kliemt¹¹, L. Koch³⁰, O. B. Kolcu^{51B,f}, B. Kopf⁴, M. Kuemmel⁴,
M. Kuessner⁴, A. Kupsc⁶⁴, M. G. Kurth^{1,52}, W. Kühn³⁰, J. J. Lane⁵⁵, J. S. Lange³⁰, P.
Larin¹⁵, L. Lavezzi^{63C}, H. Leithoff²⁸, M. Lellmann²⁸, T. Lenz²⁸, C. Li³⁹, C. H. Li³³,
Cheng Li^{60,48}, D. M. Li⁶⁸, F. Li^{1,48}, G. Li¹, H. B. Li^{1,52}, H. J. Li^{9,i}, J. L. Li⁴¹, J. Q. Li⁴, Ke Li¹,
L. K. Li¹, Lei Li³, P. L. Li^{60,48}, P. R. Li³², S. Y. Li⁵⁰, W. D. Li^{1,52}, W. G. Li¹, X. H. Li^{60,48},
X. L. Li⁴¹, Z. B. Li⁴⁹, Z. Y. Li⁴⁹, H. Liang^{1,52}, H. Liang^{60,48}, Y. F. Liang⁴⁵, Y. T. Liang²⁵,
L. Z. Liao^{1,52}, J. Libby²¹, C. X. Lin⁴⁹, B. Liu^{42,h}, B. J. Liu¹, C. X. Liu¹, D. Liu^{60,48},
D. Y. Liu^{42,h}, F. H. Liu⁴⁴, Fang Liu¹, Feng Liu⁶, H. B. Liu¹³, H. M. Liu^{1,52}, Huanhuan Liu¹,
Huihui Liu¹⁷, J. B. Liu^{60,48}, J. Y. Liu^{1,52}, K. Liu¹, K. Y. Liu³⁴, Ke Liu⁶, L. Liu^{60,48}, Q. Liu⁵²,
S. B. Liu^{60,48}, Shuai Liu⁴⁶, T. Liu^{1,52}, X. Liu³², Y. B. Liu³⁷, Z. A. Liu^{1,48,52}, Z. Q. Liu⁴¹, Y.
F. Long^{38,l}, X. C. Lou^{1,48,52}, F. X. Lu¹⁶, H. J. Lu¹⁸, J. D. Lu^{1,52}, J. G. Lu^{1,48}, X. L. Lu¹,
Y. Lu¹, Y. P. Lu^{1,48}, C. L. Luo³⁵, M. X. Luo⁶⁷, P. W. Luo⁴⁹, T. Luo^{9,i}, X. L. Luo^{1,48},
S. Lusso^{63C}, X. R. Lyu⁵², F. C. Ma³⁴, H. L. Ma¹, L. L. Ma⁴¹, M. M. Ma^{1,52}, Q. M. Ma¹,
R. Q. Ma^{1,52}, R. T. Ma⁵², X. N. Ma³⁷, X. X. Ma^{1,52}, X. Y. Ma^{1,48}, Y. M. Ma⁴¹, F. E. Maas¹⁵,
M. Maggiora^{63A,63C}, S. Maldaner²⁸, S. Malde⁵⁸, Q. A. Malik⁶², A. Mangoni^{23B}, Y. J. Mao^{38,l},

Z. P. Mao¹, S. Marcello^{63A,63C}, Z. X. Meng⁵⁴, J. G. Messchendorp³¹, G. Mezzadri^{24A},
T. J. Min³⁶, R. E. Mitchell²², X. H. Mo^{1,48,52}, Y. J. Mo⁶, N. Yu. Muchnoi^{10,d},
H. Muramatsu⁵⁶, S. Nakhoul^{11,g}, Y. Nefedov²⁹, F. Nerling^{11,g}, I. B. Nikolaev^{10,d}, Z. Ning^{1,48},
S. Nisar^{8,j}, S. L. Olsen⁵², Q. Ouyang^{1,48,52}, S. Pacetti^{23B}, X. Pan⁴⁶, Y. Pan⁵⁵, A. Pathak¹,
P. Patteri^{23A}, M. Pelizaeus⁴, H. P. Peng^{60,48}, K. Peters^{11,g}, J. Pettersson⁶⁴, J. L. Ping³⁵,
R. G. Ping^{1,52}, A. Pitka⁴, R. Poling⁵⁶, V. Prasad^{60,48}, H. Qi^{60,48}, H. R. Qi⁵⁰, M. Qi³⁶,
T. Y. Qi², S. Qian^{1,48}, W.-B. Qian⁵², Z. Qian⁴⁹, C. F. Qiao⁵², L. Q. Qin¹², X. P. Qin¹³,
X. S. Qin⁴, Z. H. Qin^{1,48}, J. F. Qiu¹, S. Q. Qu³⁷, K. H. Rashid⁶², K. Ravindran²¹,
C. F. Redmer²⁸, A. Rivetti^{63C}, V. Rodin³¹, M. Rolo^{63C}, G. Rong^{1,52}, Ch. Rosner¹⁵,
M. Rump⁵⁷, A. Sarantsev^{29,e}, M. Savrie^{24B}, Y. Schelhaas²⁸, C. Schnier⁴, K. Schoenning⁶⁴,
D. C. Shan⁴⁶, W. Shan¹⁹, X. Y. Shan^{60,48}, M. Shao^{60,48}, C. P. Shen², P. X. Shen³⁷,
X. Y. Shen^{1,52}, H. C. Shi^{60,48}, R. S. Shi^{1,52}, X. Shi^{1,48}, X. D Shi^{60,48}, J. J. Song⁴¹,
Q. Q. Song^{60,48}, W. M. Song²⁷, Y. X. Song^{38,l}, S. Sosio^{63A,63C}, S. Spataro^{63A,63C}, F. F.
Sui⁴¹, G. X. Sun¹, J. F. Sun¹⁶, L. Sun⁶⁵, S. S. Sun^{1,52}, T. Sun^{1,52}, W. Y. Sun³⁵,
Y. J. Sun^{60,48}, Y. K Sun^{60,48}, Y. Z. Sun¹, Z. T. Sun¹, Y. H. Tan⁶⁵, Y. X. Tan^{60,48},
C. J. Tang⁴⁵, G. Y. Tang¹, J. Tang⁴⁹, V. Thoren⁶⁴, B. Tsednee²⁶, I. Uman^{51D}, B. Wang¹,
B. L. Wang⁵², C. W. Wang³⁶, D. Y. Wang^{38,l}, H. P. Wang^{1,52}, K. Wang^{1,48}, L. L. Wang¹,
M. Wang⁴¹, M. Z. Wang^{38,l}, Meng Wang^{1,52}, W. H. Wang⁶⁵, W. P. Wang^{60,48}, X. Wang^{38,l},
X. F. Wang³², X. L. Wang^{9,i}, Y. Wang⁴⁹, Y. Wang^{60,48}, Y. D. Wang¹⁵, Y. F. Wang^{1,48,52},
Y. Q. Wang¹, Z. Wang^{1,48}, Z. Y. Wang¹, Ziyi Wang⁵², Zongyuan Wang^{1,52}, D. H. Wei¹²,
P. Weidenkaff²⁸, F. Weidner⁵⁷, S. P. Wen¹, D. J. White⁵⁵, U. Wiedner⁴, G. Wilkinson⁵⁸,
M. Wolke⁶⁴, L. Wollenberg⁴, J. F. Wu^{1,52}, L. H. Wu¹, L. J. Wu^{1,52}, X. Wu^{9,i}, Z. Wu^{1,48},
L. Xia^{60,48}, H. Xiao^{9,i}, S. Y. Xiao¹, Y. J. Xiao^{1,52}, Z. J. Xiao³⁵, X. H. Xie^{38,l}, Y. G. Xie^{1,48},
Y. H. Xie⁶, T. Y. Xing^{1,52}, X. A. Xiong^{1,52}, G. F. Xu¹, J. J. Xu³⁶, Q. J. Xu¹⁴, W. Xu^{1,52},
X. P. Xu⁴⁶, L. Yan^{9,i}, L. Yan^{63A,63C}, W. B. Yan^{60,48}, W. C. Yan⁶⁸, Xu Yan⁴⁶, H. J. Yang^{42,h},
H. X. Yang¹, L. Yang⁶⁵, R. X. Yang^{60,48}, S. L. Yang^{1,52}, Y. H. Yang³⁶, Y. X. Yang¹²,
Yifan Yang^{1,52}, Zhi Yang²⁵, M. Ye^{1,48}, M. H. Ye⁷, J. H. Yin¹, Z. Y. You⁴⁹, B. X. Yu^{1,48,52},
C. X. Yu³⁷, G. Yu^{1,52}, J. S. Yu^{20,m}, T. Yu⁶¹, C. Z. Yuan^{1,52}, W. Yuan^{63A,63C}, X. Q. Yuan^{38,l},
Y. Yuan¹, Z. Y. Yuan⁴⁹, C. X. Yue³³, A. Yuncu^{51B,a}, A. A. Zafar⁶², Y. Zeng^{20,m},
B. X. Zhang¹, Guangyi Zhang¹⁶, H. H. Zhang⁴⁹, H. Y. Zhang^{1,48}, J. L. Zhang⁶⁶,
J. Q. Zhang⁴, J. W. Zhang^{1,48,52}, J. Y. Zhang¹, J. Z. Zhang^{1,52}, Jianyu Zhang^{1,52},
Jiawei Zhang^{1,52}, L. Zhang¹, Lei Zhang³⁶, S. Zhang⁴⁹, S. F. Zhang³⁶, T. J. Zhang^{42,h},
X. Y. Zhang⁴¹, Y. Zhang⁵⁸, Y. H. Zhang^{1,48}, Y. T. Zhang^{60,48}, Yan Zhang^{60,48}, Yao Zhang¹,
Yi Zhang^{9,i}, Z. H. Zhang⁶, Z. Y. Zhang⁶⁵, G. Zhao¹, J. Zhao³³, J. Y. Zhao^{1,52}, J. Z. Zhao^{1,48},
Lei Zhao^{60,48}, Ling Zhao¹, M. G. Zhao³⁷, Q. Zhao¹, S. J. Zhao⁶⁸, Y. B. Zhao^{1,48},
Y. X. Zhao Zhao²⁵, Z. G. Zhao^{60,48}, A. Zhemchugov^{29,b}, B. Zheng⁶¹, J. P. Zheng^{1,48},
Y. Zheng^{38,l}, Y. H. Zheng⁵², B. Zhong³⁵, C. Zhong⁶¹, L. P. Zhou^{1,52}, Q. Zhou^{1,52}, X. Zhou⁶⁵,
X. K. Zhou⁵², X. R. Zhou^{60,48}, A. N. Zhu^{1,52}, J. Zhu³⁷, K. Zhu¹, K. J. Zhu^{1,48,52}, S. H. Zhu⁵⁹,
W. J. Zhu³⁷, X. L. Zhu⁵⁰, Y. C. Zhu^{60,48}, Z. A. Zhu^{1,52}, B. S. Zou¹, J. H. Zou¹

(BESIII Collaboration)

¹ *Institute of High Energy Physics, Beijing 100049, People's Republic of China*

² *Beihang University, Beijing 100191, People's Republic of China*

³ *Beijing Institute of Petrochemical Technology, Beijing 102617, People's Republic of China*

⁴ *Bochum Ruhr-University, D-44780 Bochum, Germany*

⁵ *Carnegie Mellon University, Pittsburgh, Pennsylvania 15213, USA*

⁶ *Central China Normal University, Wuhan 430079, People's Republic of China*

⁷ *China Center of Advanced Science and Technology, Beijing 100190, People's Republic of China*

- ⁸ COMSATS University Islamabad, Lahore Campus, Defence Road, Off Raiwind Road, 54000 Lahore, Pakistan
- ⁹ Fudan University, Shanghai 200443, People's Republic of China
- ¹⁰ G.I. Budker Institute of Nuclear Physics SB RAS (BINP), Novosibirsk 630090, Russia
- ¹¹ GSI Helmholtzcentre for Heavy Ion Research GmbH, D-64291 Darmstadt, Germany
- ¹² Guangxi Normal University, Guilin 541004, People's Republic of China
- ¹³ Guangxi University, Nanning 530004, People's Republic of China
- ¹⁴ Hangzhou Normal University, Hangzhou 310036, People's Republic of China
- ¹⁵ Helmholtz Institute Mainz, Johann-Joachim-Becher-Weg 45, D-55099 Mainz, Germany
- ¹⁶ Henan Normal University, Xinxiang 453007, People's Republic of China
- ¹⁷ Henan University of Science and Technology, Luoyang 471003, People's Republic of China
- ¹⁸ Huangshan College, Huangshan 245000, People's Republic of China
- ¹⁹ Hunan Normal University, Changsha 410081, People's Republic of China
- ²⁰ Hunan University, Changsha 410082, People's Republic of China
- ²¹ Indian Institute of Technology Madras, Chennai 600036, India
- ²² Indiana University, Bloomington, Indiana 47405, USA
- ²³ (A)INFN Laboratori Nazionali di Frascati, I-00044, Frascati, Italy; (B)INFN and University of Perugia, I-06100, Perugia, Italy
- ²⁴ (A)INFN Sezione di Ferrara, I-44122, Ferrara, Italy; (B)University of Ferrara, I-44122, Ferrara, Italy
- ²⁵ Institute of Modern Physics, Lanzhou 730000, People's Republic of China
- ²⁶ Institute of Physics and Technology, Peace Ave. 54B, Ulaanbaatar 13330, Mongolia
- ²⁷ Jilin University, Changchun 130012, People's Republic of China
- ²⁸ Johannes Gutenberg University of Mainz, Johann-Joachim-Becher-Weg 45, D-55099 Mainz, Germany
- ²⁹ Joint Institute for Nuclear Research, 141980 Dubna, Moscow region, Russia
- ³⁰ Justus-Liebig-Universitaet Giessen, II. Physikalisches Institut, Heinrich-Buff-Ring 16, D-35392 Giessen, Germany
- ³¹ KVI-CART, University of Groningen, NL-9747 AA Groningen, The Netherlands
- ³² Lanzhou University, Lanzhou 730000, People's Republic of China
- ³³ Liaoning Normal University, Dalian 116029, People's Republic of China
- ³⁴ Liaoning University, Shenyang 110036, People's Republic of China
- ³⁵ Nanjing Normal University, Nanjing 210023, People's Republic of China
- ³⁶ Nanjing University, Nanjing 210093, People's Republic of China
- ³⁷ Nankai University, Tianjin 300071, People's Republic of China
- ³⁸ Peking University, Beijing 100871, People's Republic of China
- ³⁹ Qufu Normal University, Qufu 273165, People's Republic of China
- ⁴⁰ Shandong Normal University, Jinan 250014, People's Republic of China
- ⁴¹ Shandong University, Jinan 250100, People's Republic of China
- ⁴² Shanghai Jiao Tong University, Shanghai 200240, People's Republic of China
- ⁴³ Shanxi Normal University, Linfen 041004, People's Republic of China
- ⁴⁴ Shanxi University, Taiyuan 030006, People's Republic of China
- ⁴⁵ Sichuan University, Chengdu 610064, People's Republic of China
- ⁴⁶ Soochow University, Suzhou 215006, People's Republic of China
- ⁴⁷ Southeast University, Nanjing 211100, People's Republic of China
- ⁴⁸ State Key Laboratory of Particle Detection and Electronics, Beijing 100049, Hefei 230026, People's Republic of China
- ⁴⁹ Sun Yat-Sen University, Guangzhou 510275, People's Republic of China

- ⁵⁰ *Tsinghua University, Beijing 100084, People's Republic of China*
- ⁵¹ *(A)Ankara University, 06100 Tandogan, Ankara, Turkey; (B)Istanbul Bilgi University, 34060 Eyup, Istanbul, Turkey; (C)Uludag University, 16059 Bursa, Turkey; (D)Near East University, Nicosia, North Cyprus, Mersin 10, Turkey*
- ⁵² *University of Chinese Academy of Sciences, Beijing 100049, People's Republic of China*
- ⁵³ *University of Hawaii, Honolulu, Hawaii 96822, USA*
- ⁵⁴ *University of Jinan, Jinan 250022, People's Republic of China*
- ⁵⁵ *University of Manchester, Oxford Road, Manchester, M13 9PL, United Kingdom*
- ⁵⁶ *University of Minnesota, Minneapolis, Minnesota 55455, USA*
- ⁵⁷ *University of Muenster, Wilhelm-Klemm-Str. 9, 48149 Muenster, Germany*
- ⁵⁸ *University of Oxford, Keble Rd, Oxford, UK OX13RH*
- ⁵⁹ *University of Science and Technology Liaoning, Anshan 114051, People's Republic of China*
- ⁶⁰ *University of Science and Technology of China, Hefei 230026, People's Republic of China*
- ⁶¹ *University of South China, Hengyang 421001, People's Republic of China*
- ⁶² *University of the Punjab, Lahore-54590, Pakistan*
- ⁶³ *(A)University of Turin, I-10125, Turin, Italy; (B)University of Eastern Piedmont, I-15121, Alessandria, Italy; (C)INFN, I-10125, Turin, Italy*
- ⁶⁴ *Uppsala University, Box 516, SE-75120 Uppsala, Sweden*
- ⁶⁵ *Wuhan University, Wuhan 430072, People's Republic of China*
- ⁶⁶ *Xinyang Normal University, Xinyang 464000, People's Republic of China*
- ⁶⁷ *Zhejiang University, Hangzhou 310027, People's Republic of China*
- ⁶⁸ *Zhengzhou University, Zhengzhou 450001, People's Republic of China*
- ^a *Also at Bogazici University, 34342 Istanbul, Turkey*
- ^b *Also at the Moscow Institute of Physics and Technology, Moscow 141700, Russia*
- ^c *Also at the Functional Electronics Laboratory, Tomsk State University, Tomsk, 634050, Russia*
- ^d *Also at the Novosibirsk State University, Novosibirsk, 630090, Russia*
- ^e *Also at the NRC "Kurchatov Institute", PNPI, 188300, Gatchina, Russia*
- ^f *Also at Istanbul Arel University, 34295 Istanbul, Turkey*
- ^g *Also at Goethe University Frankfurt, 60323 Frankfurt am Main, Germany*
- ^h *Also at Key Laboratory for Particle Physics, Astrophysics and Cosmology, Ministry of Education; Shanghai Key Laboratory for Particle Physics and Cosmology; Institute of Nuclear and Particle Physics, Shanghai 200240, People's Republic of China*
- ⁱ *Also at Key Laboratory of Nuclear Physics and Ion-beam Application (MOE) and Institute of Modern Physics, Fudan University, Shanghai 200443, People's Republic of China*
- ^j *Also at Harvard University, Department of Physics, Cambridge, MA, 02138, USA*
- ^k *Currently at: Institute of Physics and Technology, Peace Ave.54B, Ulaanbaatar 13330, Mongolia*
- ^l *Also at State Key Laboratory of Nuclear Physics and Technology, Peking University, Beijing 100871, People's Republic of China*
- ^m *School of Physics and Electronics, Hunan University, Changsha 410082, China*

ABSTRACT: We measure the branching fractions for seven D_s^+ two-body decays to pseudo-scalar mesons, by analyzing data collected at $\sqrt{s} = 4.178 \sim 4.226$ GeV with the BESIII detector at the BEPCII collider. The branching fractions are determined to be

$$\begin{aligned}
\mathcal{B}(D_s^+ \rightarrow K^+\eta') &= (2.68 \pm 0.17 \pm 0.17 \pm 0.08) \times 10^{-3}, \\
\mathcal{B}(D_s^+ \rightarrow \eta'\pi^+) &= (37.8 \pm 0.4 \pm 2.1 \pm 1.2) \times 10^{-3}, \\
\mathcal{B}(D_s^+ \rightarrow K^+\eta) &= (1.62 \pm 0.10 \pm 0.03 \pm 0.05) \times 10^{-3}, \\
\mathcal{B}(D_s^+ \rightarrow \eta\pi^+) &= (17.41 \pm 0.18 \pm 0.27 \pm 0.54) \times 10^{-3}, \\
\mathcal{B}(D_s^+ \rightarrow K^+K_S^0) &= (15.02 \pm 0.10 \pm 0.27 \pm 0.47) \times 10^{-3}, \\
\mathcal{B}(D_s^+ \rightarrow K_S^0\pi^+) &= (1.109 \pm 0.034 \pm 0.023 \pm 0.035) \times 10^{-3}, \\
\mathcal{B}(D_s^+ \rightarrow K^+\pi^0) &= (0.748 \pm 0.049 \pm 0.018 \pm 0.023) \times 10^{-3},
\end{aligned}$$

where the first uncertainties are statistical, the second are systematic, and the third are from external input branching fraction of the normalization mode $D_s^+ \rightarrow K^+K^-\pi^+$. Precision of our measurements is significantly improved compared with that of the current world average values.

Contents

1	INTRODUCTION	1
2	BESIII DETECTOR AND MONTE CARLO SIMULATION	2
3	MEASUREMENT METHOD	3
4	EVENT SELECTION	3
5	SIGNAL YIELD AND BRANCHING FRACTION	5
6	SYSTEMATIC UNCERTAINTY	6
7	SUMMARY AND DISCUSSION	10

1 INTRODUCTION

Among the hadronic decays of the strange-charmed meson D_s^+ , the theoretical treatment based on QCD-inspired models of its decays into two pseudoscalar mesons ($D_s^+ \rightarrow PP'$) is the cleanest [1, 2]. Precision measurements of these decay rates can provide crucial calibrations to different theoretical models [1–5]. For each decay branching fraction (BF) listed in Table 1, the precision of current measurements listed by the Particle Data Group (PDG) [6] is still not good enough to test theoretical models. Hence, more precise and independent measurements are desired to further improve our understanding of QCD dynamics in charm physics.

In 2019, LHCb discovered CP violation in $D^0 \rightarrow \pi^+\pi^-$ and $D^0 \rightarrow K^+K^-$ decays with a significance of 5.3σ [7], providing stringent constraints on theoretical approaches to CP violation in the charm sector [1, 4, 8]. For the strange-charmed meson D_s^+ , there are theoretical predictions for the CP asymmetries of the singly Cabibbo-suppressed (SCS) decay modes, which rely on the potential effect of SU(3) symmetry breaking [3, 9]. However, the current world average results, as shown in Table 1, suffer from large uncertainties and are thus insensitive to SU(3) breaking. More precise measurements of the BFs for the SCS modes in $D_s^+ \rightarrow PP'$ will help to explore SU(3) symmetry breaking in D_s^+ decays [3, 9]. As a result, more reliable theoretical predictions of CP asymmetries in the D_s^+ SCS hadronic decays can be achieved.

In this work, we measure the BFs for seven two-body hadronic decays $D_s^+ \rightarrow PP'$: $D_s^+ \rightarrow K^+\eta'$, $\eta'\pi^+$, $K^+\eta$, $\eta\pi^+$, $K^+K_S^0$, $K_S^0\pi^+$ and $K^+\pi^0$. These decay modes were previously measured by CLEO [10–12]. The analysis is carried out in the process of $e^+e^- \rightarrow D_s^+D_s^{*-} + c.c. \rightarrow \gamma D_s^+D_s^-$ based on data samples collected at the center-of-mass energies $\sqrt{s} = 4.178, 4.189, 4.199, 4.209, 4.219$ and 4.226 GeV, corresponding to the integrated luminosities of 3189.0, 526.7, 526.0, 517.1, 514.6 and 1091.7 pb^{-1} , respectively [13, 14].

A partial reconstruction technique is adopted: only one D_s^\pm , decaying into the PP' mode, is detected along with a soft photon from $D_s^{*\pm}(D_s^{*\mp})$; the other D_s^\mp is not used. The BFs are measured relative to the normalization mode $D_s^+ \rightarrow K^+K^-\pi^+$. In the context, charge conjugate modes are always implied, unless explicitly mentioned.

Table 1. Comparisons of the D_s^+ decay BFs between the world average results from PDG [6] and calculations from different theoretical models (in unit of 10^{-3}).

Decay	PDG	Cheng <i>et al.</i> [3]		Cheng <i>et al.</i>	Yu <i>et al.</i>	Li <i>et al.</i>	Wang <i>et al.</i>
	[6]	SU(3)	SU(3)-breaking	[1]	[2]	[4]	[5]
$K^+\eta'$	1.8 ± 0.6	1.23 ± 0.06	1.49 ± 0.08	1.07 ± 0.17	1.4 ± 0.4	1.92	3.1 ± 0.4
$\eta'\pi^+$	39.4 ± 2.5	-	-	38.2 ± 3.6	46 ± 6	34.4	46.7 ± 6.2
$K^+\eta$	1.77 ± 0.35	0.91 ± 0.03	0.86 ± 0.03	0.78 ± 0.09	0.8 ± 0.5	1.00	0.91 ± 0.20
$\eta\pi^+$	17.0 ± 0.9	-	-	18.2 ± 3.2	19 ± 5	16.5	19.6 ± 4.4
$K^+K_S^0$	15.0 ± 0.5	-	-	14.85 ± 1.60	15.0 ± 4.5	15.0	15.0 ± 1.6
$K_S^0\pi^+$	1.22 ± 0.06	1.20 ± 0.04	1.27 ± 0.04	1.365 ± 0.130	1.4 ± 0.3	1.105	1.04 ± 0.13
$K^+\pi^0$	0.63 ± 0.21	0.86 ± 0.04	0.56 ± 0.02	0.86 ± 0.09	0.5 ± 0.2	0.67	0.69 ± 0.03

2 BESIII DETECTOR AND MONTE CARLO SIMULATION

The BESIII detector is a magnetic spectrometer [15] located at BEPCII [16]. The cylindrical core of the BESIII detector consists of a helium-based main drift chamber (MDC), a plastic scintillator time-of-flight system (TOF), and a CsI(Tl) electromagnetic calorimeter (EMC), which are all enclosed in a superconducting solenoidal magnet providing a 1.0 T magnetic field. The solenoid is supported by an octagonal flux-return yoke with resistive plate counter muon tracker modules interleaved with steel. The acceptance of charged particles and photons is 93% over 4π solid angle. The charged-particle momentum resolution at 1 GeV/ c is 0.5%, and the ionization energy loss dE/dx resolution is 6% for the electrons from Bhabha scattering. The EMC measures photon energies with a resolution of 2.5% (5%) at 1 GeV in the barrel (end cap) region. The time resolution of the TOF barrel part is 68 ps, while that of the end cap part is 110 ps. The end cap TOF system was upgraded in 2015 with multi-gap resistive plate chamber technology, providing a time resolution of 60 ps [17, 18]. Only the 4.226 GeV data was taken before this upgrade.

Simulated data samples, produced with the GEANT4-based [19] Monte Carlo (MC) package which includes the geometric description of the BESIII detector and the detector response, are used to determine the detection efficiency and to estimate the backgrounds. The simulation includes the beam energy spread and initial state radiation in the e^+e^- annihilations modeled with the generator KKMC [20, 21]. In order to study the backgrounds, generic MC samples consisting of open-charm states, radiative return to J/ψ and $\psi(2S)$, and continuum processes of $q\bar{q}$ ($q = u, d, s$), along with Bhabha scattering, $\mu^+\mu^-$, $\tau^+\tau^-$, and $\gamma\gamma$ events are generated. The known decay modes are modeled with EVTGEN [22, 23] using BFs taken from PDG [6], and the remaining unknown decays from the charmonium states are treated with LUNDCHARM [24, 25]. Final state radiation (FSR) from charged

final state particles is incorporated with the PHOTOS package [26]. The signal MC samples of $e^+e^- \rightarrow D_s^{*\pm} D_s^\mp$ with a D_s^+ meson decaying to the signal decay modes together with a D_s^- decaying inclusively are generated with CONEXC [27].

3 MEASUREMENT METHOD

In this analysis, a candidate D_s^+ meson is reconstructed by the combination of the detected final-state particles. With current precision, CP violation is negligible, which means the BFs for D_s^+ decays to the mode i^+ , $\mathcal{B}^{i^+} \equiv \mathcal{B}(D_s^+ \rightarrow i^+)$, and for D_s^- decays to the mode i^- , \mathcal{B}^{i^-} , are equal. Therefore, we denote $\mathcal{B}^{i^+} = \mathcal{B}^{i^-} = \mathcal{B}^i$. The yield, n^i , of the observed $D_s^+ \rightarrow i$ signal events at all six energy points can be written as

$$n^i = 2N^{D_s^{*+}D_s^-} \cdot \mathcal{B}^i \cdot \mathcal{B}_{\text{final-state}}^i \cdot \bar{\varepsilon}^i, \quad (3.1)$$

where $N^{D_s^{*+}D_s^-}$ is the total number of $D_s^{*+}D_s^-$ pairs produced in all the data samples. For mode i , $\mathcal{B}_{\text{final-state}}^i$ is the combined BF from the i state to the observed final state (those are described in Section 4), and $\bar{\varepsilon}^i$ is average detection efficiency for the whole data set, which is given as

$$\bar{\varepsilon}^i = \frac{\sum_{k=1}^6 L_k \cdot \sigma_k \cdot \varepsilon_k^i}{\sum_{k=1}^6 L_k \cdot \sigma_k}. \quad (3.2)$$

Here, L_k is the integrated luminosity, σ_k is the observed cross section and ε_k^i is the detection efficiency at the k -th energy point.

The absolute BF of the normalization mode decay, $D_s^+ \rightarrow K^+K^-\pi^+$, is denoted by $\mathcal{B}^{K^+K^-\pi^+}$ and is taken from PDG [6]. Based on Eq. (3.1), the relative BF for the signal mode $D_s^+ \rightarrow i$ is

$$R^i = \frac{\mathcal{B}^i}{\mathcal{B}^{K^+K^-\pi^+}} = \frac{n^i \cdot \bar{\varepsilon}^{K^+K^-\pi^+}}{n^{K^+K^-\pi^+} \cdot \bar{\varepsilon}^i \cdot \mathcal{B}_{\text{final-state}}^i}. \quad (3.3)$$

The absolute BF \mathcal{B}^i is obtained by

$$\mathcal{B}^i = R^i \cdot \mathcal{B}^{K^+K^-\pi^+}. \quad (3.4)$$

4 EVENT SELECTION

Charged tracks are reconstructed from hits in the MDC. Except for the tracks used to reconstruct the K_S^0 meson, the distances of closest approach to the interaction point are required to satisfy $R_{xy} < 1.0$ cm in the xy plane perpendicular to the z direction of the MDC and $R_z < 10.0$ cm along the z direction. The track polar angle θ must satisfy $|\cos \theta| < 0.93$. For particle identification (PID) of charged tracks, measurements of dE/dx and the flight time measured by the TOF are combined to form a likelihood $L(h)$ ($h = \pi, K$) for each hadron hypothesis. Tracks are identified as charged pions when the PID likelihoods of pions are larger than those of kaons, $L(\pi) > L(K)$, while tracks with $L(K) > L(\pi)$ are identified as kaons.

Shower clusters with no association to any charged tracks in the EMC crystals will be identified as photon candidates when the following requirements are fulfilled: the measured EMC time is within $0 \leq t \leq 700$ ns of the event start time to suppress the electronic noise and showers unrelated to the events; the deposited energy is larger than 25 MeV in the barrel ($|\cos\theta| < 0.80$) and larger than 50 MeV in the end cap ($0.86 < |\cos\theta| < 0.92$). Additionally, the angle between a photon candidate and the nearest charged track must be larger than 10° to prevent contamination from hadronic showers.

The π^0 and η meson candidates are reconstructed from photon pairs with the invariant mass $M(\gamma\gamma)$ within $[0.120, 0.145]$ GeV/ c^2 and $[0.510, 0.560]$ GeV/ c^2 , respectively. In order to improve the momentum resolution, a kinematic fit constraining the reconstructed π^0 (η) mass to its nominal mass [6] is applied and the fitted four-momentum of the π^0 (η) meson is used for further analysis. The η' meson candidates are reconstructed from $\pi^+\pi^-\eta$ with an $M(\pi^+\pi^-\eta)$ invariant mass requirement of $[0.945, 0.970]$ GeV/ c^2 .

Candidate K_S^0 mesons are reconstructed from two oppositely charged tracks, with no PID requirement; these tracks are required to satisfy the polar angle requirement $|\cos\theta| < 0.93$ and $R_{xy} < 20$ cm. Furthermore, there is usually a detectable displacement before the decay of K_S^0 meson due to its relatively long lifetime. Therefore, the decay length and corresponding uncertainty of K_S^0 candidates are required to satisfy $L/\sigma_L > 2$, which suppresses prompt $\pi^+\pi^-$ combinatorial background [28]. The K_S^0 meson candidates with an invariant mass $M(\pi^+\pi^-)$ within the mass window $[0.491, 0.505]$ GeV/ c^2 are retained.

For a specific D_s^+ decay mode, the D_s^+ signal candidates are formed by combining all the detected final-state particles. In addition, a radiative photon from the $D_s^{*\pm}$ decay must be detected. Among all the γD_s^+ combinations in the event, the one with the minimal $|\Delta\mathbb{E}|$ is kept for subsequent analysis only, where $\Delta\mathbb{E}$ is the difference between the center-of-mass energy $E_0 \equiv \sqrt{s}$ and the total energy of $\gamma D_s^+ D_s^-$ in the center-of-mass frame of the e^+e^- beams

$$\Delta\mathbb{E} = (E_{D_s^+} + E_\gamma + E_{\text{rec}}) - E_0. \quad (4.1)$$

Here $E_{D_s^+}$ and E_γ are the energies of reconstructed D_s^+ and γ from $D_s^{*\pm}$, respectively. E_{rec} is the energy of the recoiled D_s^- , calculated using

$$E_{\text{rec}} = \sqrt{|-(\vec{p}_{D_s^+} + \vec{p}_\gamma)|^2 + m_{D_s^-}^2}, \quad (4.2)$$

where $\vec{p}_{D_s^+}$ is the total momentum of the detected D_s^+ , \vec{p}_γ is the momentum of the radiative photon γ , and $m_{D_s^-}$ is the nominal mass of the D_s^- [6]. For a correctly reconstructed D_s^+ candidate, $\Delta\mathbb{E}$ is expected to be around zero. Therefore, candidates will be rejected when they fail the requirements of $\Delta\mathbb{E}$ for each decay mode, as shown in Table 2, which correspond to the $\pm 3\sigma$ regions of the signal $\Delta\mathbb{E}$ distributions. To further improve the kinematic resolutions of the final states, a kinematic fit is performed to constrain the recoil mass of the $D_s^+\gamma$, $M_{\text{rec}}(D_s^+\gamma)$, to the nominal mass of the D_s^- . According to the kinematic fit, the four momenta of all the final-state particles are updated.

As an example, data for $D_s^+ \rightarrow K^+\pi^0$ is shown in Fig. 1; the two-dimensional distribution of the recoil mass $M_{\text{rec}}(D_s^+)$ and the invariant mass $M(D_s^+\gamma)$ depicts the two resonance structures of the processes. The horizontal band corresponds to $e^+e^- \rightarrow D_s^{*+}D_s^- \rightarrow$

Table 2. Summary of the requirements of ΔE , $M_{\text{rec}}(D_s^+)$ and $M(D_s^+\gamma)$ for each $D_s^+ \rightarrow PP'$ decay mode and the normalization mode.

Decay	$\Delta E(\text{GeV})$	$M_{\text{rec}}(D_s^+)(\text{GeV}/c^2)$	$M(D_s^+\gamma)(\text{GeV}/c^2)$
$K^+\eta'$	(-0.040, 0.025)	(2.100, 2.130)	(2.095, 2.130)
$\eta'\pi^+$	(-0.040, 0.025)	(2.100, 2.130)	(2.095, 2.130)
$K^+\eta$	(-0.045, 0.025)	(2.100, 2.130)	(2.095, 2.130)
$\eta\pi^+$	(-0.045, 0.025)	(2.100, 2.130)	(2.095, 2.130)
$K^+K_S^0$	(-0.040, 0.020)	(2.100, 2.130)	(2.100, 2.130)
$K_S^0\pi^+$	(-0.040, 0.020)	(2.100, 2.130)	(2.100, 2.130)
$K^+\pi^0$	(-0.050, 0.020)	(2.100, 2.130)	(2.100, 2.130)
$K^+K^-\pi^+$	(-0.030, 0.020)	(2.100, 2.130)	(2.100, 2.130)

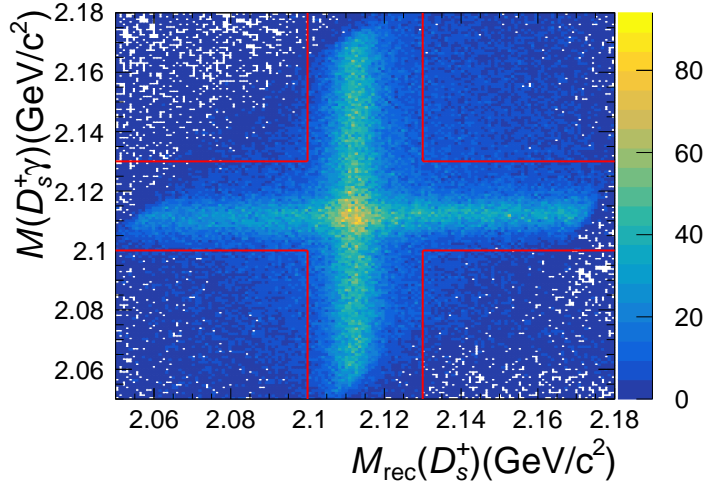


Figure 1. Two-dimensional distribution of the recoil mass of D_s^+ and the invariant mass of $D_s^+\gamma$ for the decay $D_s^+ \rightarrow K^+\pi^0$, where the solid lines denote the boundaries for the horizontal and vertical band ranges.

$\gamma D_s^+ D_s^-$, while the vertical band corresponds to $e^+e^- \rightarrow D_s^+ D_s^{*-} \rightarrow D_s^+ \gamma D_s^-$. To improve the signal-to-background ratio, we further retain only events lying in the regions of the horizontal or vertical bands defined in Table 2.

5 SIGNAL YIELD AND BRANCHING FRACTION

To extract the signal yields for the signal $D_s^+ \rightarrow PP'$ decay modes and the normalization decay mode, unbinned extended maximum likelihood fits are performed on the $M(D_s^+)$ distributions of the selected candidates in data. In each fit, the probability density function (PDF) is parameterized as the sum of signal and background PDFs. The signal PDF is a template shape formed from the signal MC sample convolved with a Gaussian function

to compensate the resolution difference between data and MC simulations. For the more common Cabibbo-favored (CF) decay modes $D_s^+ \rightarrow K^+K^-\pi^+$, $D_s^+ \rightarrow K^+K_S^0$, $D_s^+ \rightarrow \eta\pi^+$, $D_s^+ \rightarrow \eta'\pi^+$ and the SCS decay $D_s^+ \rightarrow K^+\pi^0$, the Gaussian parameters are left free. For the low-yield SCS decays $D_s^+ \rightarrow K_S^0\pi^+$, $D_s^+ \rightarrow K^+\eta$ and $D_s^+ \rightarrow K^+\eta'$, the Gaussian parameters are fixed at the values obtained from the corresponding fits to the CF decay modes $D_s^+ \rightarrow K^+K_S^0$, $D_s^+ \rightarrow \eta\pi^+$ and $D_s^+ \rightarrow \eta'\pi^+$, respectively, since the kaons and pions have almost the same kinematics. According to the background study using inclusive MC samples, peaking backgrounds are present for the modes of $D_s^+ \rightarrow \eta'\pi^+$, $D_s^+ \rightarrow K^+K_S^0$ and $D_s^+ \rightarrow K_S^0\pi^+$. The peaking backgrounds are modeled in the fit with the MC-determined shape and size. The fractions of the peaking background in the total event yields are estimated to be 2.0%, 1.4% and 1.6% for $D_s^+ \rightarrow \eta'\pi^+$, $D_s^+ \rightarrow K^+K_S^0$ and $D_s^+ \rightarrow K_S^0\pi^+$, respectively. The non-peaking background components are described with linear functions and second-order Chebychev functions for the CF and SCS decay modes, respectively. The fits are presented in Fig. 2, and the numerical results of the signal yields are listed in Table 3. The relative and absolute BFs, calculated with the average detection efficiencies obtained from the signal MC simulations, are summarized in Table 3.

Table 3. Summary of the signal yields, average detection efficiencies, relative BFs and absolute BFs of individual signal decay modes. The first uncertainty is statistical, the second is systematic, and the third is external, from the BF of the normalization mode $D_s^+ \rightarrow K^+K^-\pi^+$ [6]. The uncertainties on efficiencies are due to the limited MC event statistics.

Decay	n^i	$\bar{\varepsilon}^i$ (%)	R^i (%)	\mathcal{B}^i (10^{-3})
$K^+\eta'$	675 ± 43	13.66 ± 0.20	$4.91 \pm 0.31 \pm 0.31$	$2.68 \pm 0.17 \pm 0.17 \pm 0.08$
$\eta'\pi^+$	9912 ± 113	14.19 ± 0.04	$69.4 \pm 0.8 \pm 3.8$	$37.8 \pm 0.4 \pm 2.1 \pm 1.2$
$K^+\eta$	1841 ± 114	26.21 ± 0.17	$2.97 \pm 0.18 \pm 0.06$	$1.62 \pm 0.10 \pm 0.03 \pm 0.05$
$\eta\pi^+$	19519 ± 192	25.86 ± 0.05	$31.94 \pm 0.33 \pm 0.49$	$17.41 \pm 0.18 \pm 0.27 \pm 0.54$
$K^+K_S^0$	35977 ± 206	31.47 ± 0.05	$27.55 \pm 0.18 \pm 0.50$	$15.02 \pm 0.10 \pm 0.27 \pm 0.47$
$K_S^0\pi^+$	2724 ± 83	32.27 ± 0.16	$2.035 \pm 0.062 \pm 0.042$	$1.109 \pm 0.034 \pm 0.023 \pm 0.035$
$K^+\pi^0$	2275 ± 149	27.96 ± 0.18	$1.373 \pm 0.090 \pm 0.033$	$0.748 \pm 0.049 \pm 0.018 \pm 0.023$
$K^+K^-\pi^+$	160262 ± 478	26.73 ± 0.02	100	54.5 ± 1.7

6 SYSTEMATIC UNCERTAINTY

The sources of systematic uncertainties considered in obtaining the relative BFs include the MC statistics, $\sigma(e^+e^- \rightarrow D_s^{*+}D_s^-)$ lineshape, shapes of invariant mass distributions for signal and background, peaking background modeling, kinematic fit, ΔE and invariant mass requirements, reconstruction efficiency estimation and quoted BFs. Table 4 summarizes all of these systematic uncertainties. Some correlated uncertainties between the signal decay modes and the reference decay mode have been partially cancelled when extracting R^i in Table 3.

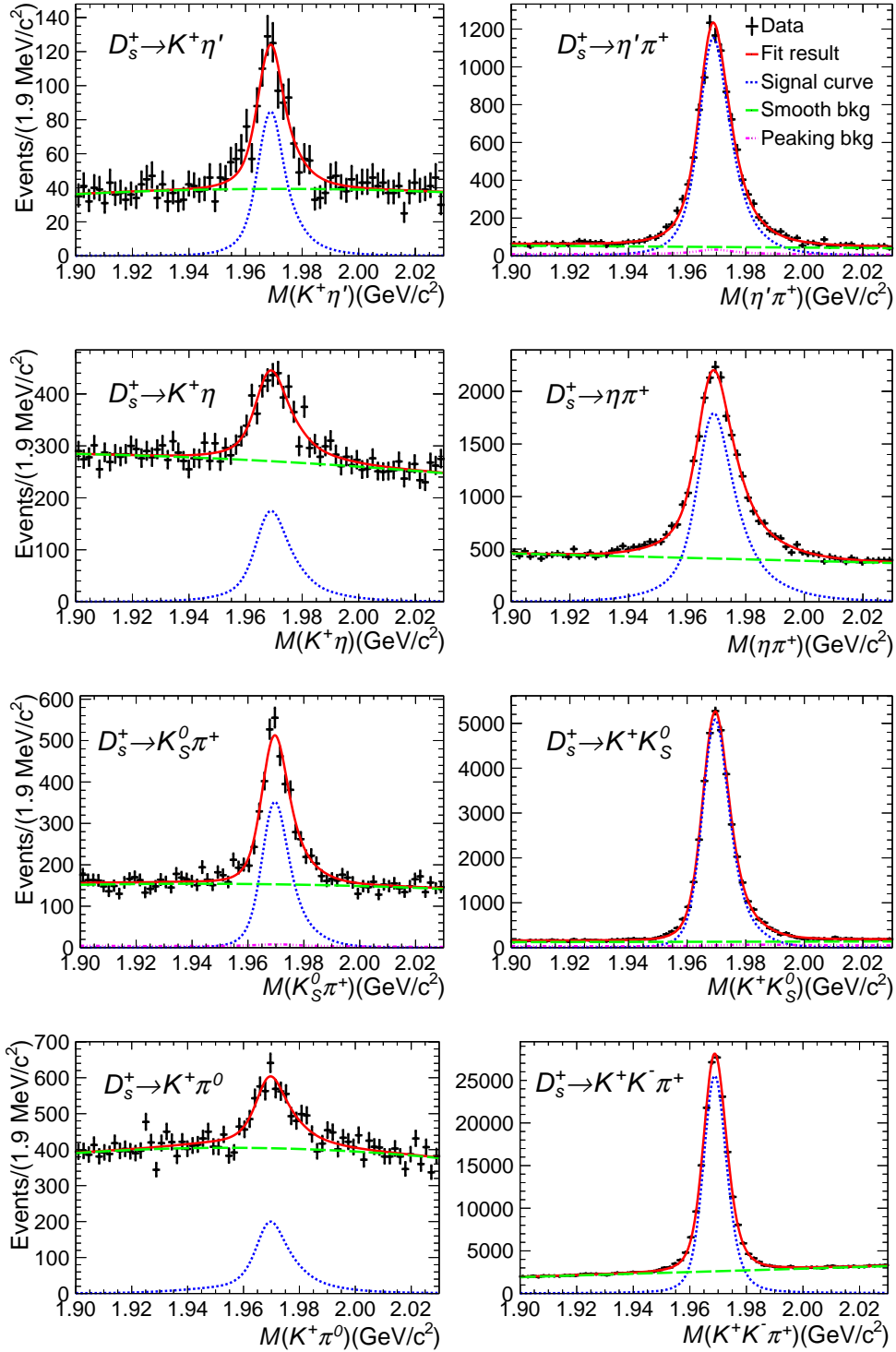


Figure 2. Fits to the invariant mass spectra of the signal candidates in data (shown as dots with error bars). The solid lines are the fit results, the dotted lines are the signal components, the long dashed lines are the non-peaking backgrounds and the dotted dashed lines are the peaking backgrounds.

Table 4. Summary of the systematic uncertainties (in unit of %) for the measurements of relative BFs . The total values are calculated by summing up all contributions in quadrature.

Source	$K^+\eta'$	$\eta'\pi^+$	$K^+\eta$	$\eta\pi^+$	$K^+K_S^0$	$K_S^0\pi^+$	$K^+\pi^0$
MC statistics	0.7	0.1	0.3	0.1	0.1	0.2	0.3
Lineshape	1.0	0.5	1.1	0.9	0.1	1.0	1.8
Signal shape	1.0	1.0	0.7	0.7	0.3	0.3	0.3
Background shape	0.0	0.3	1.0	0.2	0.0	0.8	1.4
Peaking background	-	0.8	-	-	0.0	0.1	-
Kinematic fit	0.6	0.6	0.6	0.6	0.0	0.0	0.6
ΔE and invariant masses	2.2	1.8	0.4	0.4	1.1	1.0	0.4
Reconstruction efficiency	5.4	4.6	0.2	0.5	1.4	1.2	0.0
Quoted BFs	1.7	1.7	0.5	0.5	0.1	0.1	0.0
Total	6.3	5.4	1.9	1.5	1.8	2.1	2.4

- *MC Statistics.* Average detection efficiencies are evaluated using MC simulated samples. The uncertainties due to the limited sample sizes, obtained by propagating the statistical uncertainties of the individual efficiencies at different energy points according to Eq. (3.2), are assigned as systematic uncertainties.
- $\sigma(e^+e^- \rightarrow D_s^{*+}D_s^-)$ *lineshape.* Signal PDFs and detection efficiencies have slight dependencies on the input lineshape of $\sigma(e^+e^- \rightarrow D_s^{*+}D_s^-)$. To evaluate this uncertainty, different lineshapes are used to estimate the detection efficiencies and data yields. The resulting changes in BFs are taken as systematic uncertainties.
- *Signal shape.* The uncertainties related to the signal shapes are studied using the decays $D_s^+ \rightarrow K^+\pi^0$, $D_s^+ \rightarrow \eta'\pi^+$, $D_s^+ \rightarrow \eta\pi^+$ and $D_s^+ \rightarrow K^+K_S^0$. In the nominal analysis, signal shape in the $M(D_s^+)$ distribution of the signal candidates is modeled by the signal PDF convolved with a Gaussian function. Double-Gaussian functions are used instead as convolution functions, and the resultant changes of BFs are taken as systematic uncertainties. For the low-yield SCS decays $D_s^+ \rightarrow K_S^0\pi^+$, $D_s^+ \rightarrow K^+\eta$ and $D_s^+ \rightarrow K^+\eta'$ the uncertainties of the corresponding CF modes are used.
- *Background shape.* In the nominal analysis, the background shapes are described by first-order polynomial functions for the decays $D_s^+ \rightarrow \eta'\pi^+$, $D_s^+ \rightarrow \eta\pi^+$, $D_s^+ \rightarrow K^+K_S^0$ and $D_s^+ \rightarrow K^+K^-\pi^+$ and second-order polynomials for the decays $D_s^+ \rightarrow K^+\eta'$, $D_s^+ \rightarrow K^+\eta$, $D_s^+ \rightarrow K_S^0\pi^+$ and $D_s^+ \rightarrow K^+\pi^0$. To estimate the uncertainties from the background shapes, higher-order polynomials are considered as alternatives: second-order and third-order, respectively. The resulting changes of the BFs are taken as systematic uncertainties.
- *Peaking background.* The contributions to the peaking backgrounds of $D_s^+ \rightarrow K^+K_S^0$, $D_s^+ \rightarrow K_S^0\pi^+$ and $D_s^+ \rightarrow \eta'\pi^+$ are from the decays of $D^+ \rightarrow K_S^0\pi^+$ (due to K^+ and π^+ misidentification), $D_s^+ \rightarrow \pi^+\pi^+\pi^-$ and $D_s^+ \rightarrow a_1(1260)^+\eta$ ($a_1(1260)^+ \rightarrow$

$\rho^0\pi^+, \rho^0 \rightarrow \pi^+\pi^-$) [29], respectively. Their shapes and sizes are fixed according to MC simulations in the fit. The input BFs of these background processes are varied by their uncertainties and the changes in results are taken as systematic uncertainties.

- *Kinematic fit.* High-yield CF decays of $D_s^+ \rightarrow K^+K_S^0$ and $D_s^+ \rightarrow \eta\pi^+$ are used to study the uncertainty due to the kinematic fit. We perform the analysis without applying the kinematic fit. The differences from the nominal results are taken as systematic uncertainties. For the $D_s^+ \rightarrow K_S^0\pi^+$ mode the uncertainty from $D_s^+ \rightarrow K^+K_S^0$ is taken while the uncertainty from $D_s^+ \rightarrow \eta\pi^+$ is assigned to the decays with photons in the final states.
- *$\Delta\mathbb{E}$ and invariant mass requirements.* To estimate potential bias on efficiency estimations by restricting the kinematics in the selected regions, the distributions of the kinematic variables in MC simulations are smeared with Gaussian functions. The parameters of the functions are obtained by fitting the smeared MC distributions to the corresponding distributions in data. The variables $\Delta\mathbb{E}$, $M(\pi^+\pi^-)$, $M(\gamma\gamma)$, $M(\pi^+\pi^-\eta)$, $M_{\text{rec}}(D_s^+)$ and $M(D_s^+\gamma)$ are studied. Updated efficiencies based on the Gaussian-smeared MC simulations are obtained and the relative changes from the nominal efficiencies are assigned as the systematic uncertainties.
- *Reconstruction efficiency.* We consider the efficiencies of tracking and PID (K^\pm, π^\pm) and the efficiencies of intermediate particles (π^0, η, K_S^0) reconstructions, which are studied based on a series of control samples. The K^\pm and π^\pm tracking and PID efficiencies are studied using control samples of $e^+e^- \rightarrow K^+K^-\pi^+\pi^-$, $K^+K^-K^+K^-$, $K^+K^-\pi^+\pi^-\pi^0$, $\pi^+\pi^-\pi^+\pi^-$ and $\pi^+\pi^-\pi^+\pi^-\pi^0$ events [30]. A partial cancellation of the tracking and PID uncertainties in the ratio of the signal modes and the normalization mode is taken into account. The π^0 and η reconstruction efficiencies are evaluated using the double-tag $D\bar{D}$ hadronic decays $D^0 \rightarrow K^-\pi^+$, $K^-\pi^+\pi^+\pi^-$ versus $\bar{D}^0 \rightarrow K^+\pi^-\pi^0$, $K_S^0\pi^0$ [31, 32] and approximating the η behavior as similar to the π^0 . The K_S^0 reconstruction efficiency is studied with samples of $J/\psi \rightarrow K^*(892)^\pm K^\mp$, $K^*(892)^\pm \rightarrow K_S^0\pi^\pm$ and $J/\psi \rightarrow \phi K_S^0 K^\mp \pi^\pm$ [33]. To account for the different kinematics of the various signal modes, the nominal detection efficiencies are scaled based on event-by-event corrections according to the momentum-dependent efficiency differences between MC simulations and data. The appropriately averaged scaling factors are assigned as the corresponding systematic uncertainties, as given in Table 4. Here, the $D_s^+ \rightarrow K^+\eta'$ and $D_s^+ \rightarrow \eta'\pi^+$ decays suffer from large reconstruction uncertainties due to the low-momentum charged pions and η from η' decay.
- *Quoted BFs.* The nominal BFs of $K_S^0 \rightarrow \pi^+\pi^-$, $\pi^0 \rightarrow \gamma\gamma$, $\eta \rightarrow \gamma\gamma$ and $\eta' \rightarrow \eta\pi^+\pi^-$ are used and their corresponding uncertainties [6] are propagated as systematic uncertainties.

Table 5. Results of the obtained relative BFs (in unit of %). The first uncertainty is statistical, and the second is systematic.

Relative BFs	This work	PDG [6]
$\mathcal{B}(K^+\eta')/\mathcal{B}(\eta'\pi^+)$	$7.07 \pm 0.46 \pm 0.11$	4.2 ± 1.3
$\mathcal{B}(K^+\eta)/\mathcal{B}(\eta\pi^+)$	$9.31 \pm 0.58 \pm 0.10$	8.9 ± 1.6
$\mathcal{B}(K_S^0\pi^+)/\mathcal{B}(K^+K_S^0)$	$7.38 \pm 0.23 \pm 0.09$	8.12 ± 0.28
$\mathcal{B}(K^+\eta)/\mathcal{B}(K^+\eta')$	$60.6 \pm 5.4 \pm 3.6$	–
$\mathcal{B}(\eta\pi^+)/\mathcal{B}(\eta'\pi^+)$	$46.0 \pm 0.7 \pm 2.1$	–

7 SUMMARY AND DISCUSSION

The BFs for $D_s^+ \rightarrow K^+\eta'$, $D_s^+ \rightarrow \eta'\pi^+$, $D_s^+ \rightarrow K^+\eta$, $D_s^+ \rightarrow \eta\pi^+$, $D_s^+ \rightarrow K^+K_S^0$, $D_s^+ \rightarrow K_S^0\pi^+$ and $D_s^+ \rightarrow K^+\pi^0$ are measured using e^+e^- collision data collected at $\sqrt{s} = 4.178 \sim 4.226$ GeV in the BESIII experiment. The results obtained in this work are listed in Table 3 and can be compared with the results from PDG [6] as well as with theoretical predictions [1, 2, 4, 5] (Table 1). Our results are consistent with the PDG values, while the precision is three to five times better than that of previous results. In addition, our results in general agree with the available theoretical calculations [1–5] within about 3σ . However, the discrepancies from our measurements are significant for the model calculations in Ref. [1] for the modes $D_s^+ \rightarrow K^+\eta'$ and $D_s^+ \rightarrow K^+\eta$, and from the model calculations in Ref. [4] for the mode $D_s^+ \rightarrow K^+\eta$. Investigating these discrepancies should aid in further developing these QCD-derived models in charm physics.

The ratios of the BFs, $\mathcal{B}(K^+\eta')/\mathcal{B}(\eta'\pi^+)$, $\mathcal{B}(K^+\eta)/\mathcal{B}(\eta\pi^+)$, $\mathcal{B}(K_S^0\pi^+)/\mathcal{B}(K^+K_S^0)$, $\mathcal{B}(K^+\eta)/\mathcal{B}(K^+\eta')$, and $\mathcal{B}(\eta\pi^+)/\mathcal{B}(\eta'\pi^+)$, are also determined, as listed in Table 5. The partial cancellations of the systematic uncertainties from $\sigma(e^+e^- \rightarrow D_s^{*+}D_s^-)$ lineshape, signal shape, background shape, peaking background, kinematic fit, ΔE and invariant mass requirements, and reconstruction efficiency between the pairs of decay modes are considered. Our results of $\mathcal{B}(K^+\eta')/\mathcal{B}(\eta'\pi^+)$, $\mathcal{B}(K^+\eta)/\mathcal{B}(\eta\pi^+)$, $\mathcal{B}(K_S^0\pi^+)/\mathcal{B}(K^+K_S^0)$ are consistent with the PDG values within about 2σ , but the precisions are improved. Our results are also in general accord with the theoretical calculations [1–5] within about 3σ . However, our measurements are in disagreement with the model calculations in Refs. [1, 2] for the ratio $\mathcal{B}(K^+\eta')/\mathcal{B}(\eta'\pi^+)$ and with those in Refs. [1, 4] for the ratio $\mathcal{B}(K^+\eta)/\mathcal{B}(\eta\pi^+)$. The theoretical uncertainties on these ratios are expected to be reduced as well, offering more meaningful comparisons between experimental measurements and theoretical calculations.

Acknowledgments

The BESIII collaboration thanks the staff of BEPCII and the IHEP computing center for their strong support. This work is supported in part by National Natural Science Foundation of China (NSFC) under Contracts Nos. 11625523, 11635010, 11675275, 11735014, 11775027, 11822506, 11835012, 11935015, 11935016, 11935018, 11975021, 11961141012;

National Key Basic Research Program of China under Contract No. 2015CB856700; the Chinese Academy of Sciences (CAS) Large-Scale Scientific Facility Program; CAS Key Research Program of Frontier Sciences under Contracts Nos. QYZDJ-SSW-SLH003, QYZDJ-SSW-SLH040; Joint Large-Scale Scientific Facility Funds of the NSFC and CAS under Contracts Nos. U1932101, U1832207, U1732263; 100 Talents Program of CAS; National 1000 Talents Program of China; INPAC and Shanghai Key Laboratory for Particle Physics and Cosmology; The University of Chinese Academy of Sciences; The Beijing municipal government under Contract No. CIT&TCD201704047; ERC under Contract No. 758462; German Research Foundation DFG under Contracts Nos. Collaborative Research Center CRC 1044, FOR 2359; Istituto Nazionale di Fisica Nucleare, Italy; Ministry of Development of Turkey under Contract No. DPT2006K-120470; National Science and Technology fund; STFC (United Kingdom); The Knut and Alice Wallenberg Foundation (Sweden) under Contract No. 2016.0157; The Royal Society, UK under Contracts Nos. DH140054, DH160214; The Swedish Research Council; U. S. Department of Energy under Contracts Nos. DE-FG02-05ER41374, DE-SC-0012069.

References

- [1] H. Y. Cheng and C. W. Chiang, *Two-body hadronic charmed meson decays*, *Phys. Rev. D* **81** (2010) 074021. [arXiv:1001.0987]
- [2] F. S. Yu, X. X. Wang and C. D. Lu, *Nonleptonic Two Body Decays of Charmed Mesons*, *Phys. Rev. D* **84** (2011) 074019. [arXiv:1101.4714]
- [3] H. Y. Cheng and C. W. Chiang, *Revisiting CP violation in $D \rightarrow PP$ and VP decays*, *Phys. Rev. D* **100** (2019) 093002. [arXiv:1909.03063]
- [4] H. n. Li, C. D. Lu and F. S. Yu, *Branching ratios and direct CP asymmetries in $D \rightarrow PP$ decays*, *Phys. Rev. D* **86** (2012) 036012. [arXiv:1203.3120]
- [5] D. Wang, F. S. Yu, P. F. Guo and H. Y. Jiang, *$K_S^0 - K_L^0$ asymmetries in D -meson decays*, *Phys. Rev. D* **95** (2017) 073007. [arXiv:1701.07173]
- [6] M. Tanabashi *et al.* [Particle Data Group], *Review of Particle Physics*, *Phys. Rev. D* **98** (2018) 030001 and the 2019 online update.
- [7] R. Aaij *et al.* [LHCb Collaboration], *Observation of CP violation in charm decays*, *Phys. Rev. Lett.* **122** (2019) 211803. [arXiv:1903.08726]
- [8] Miroslav Saur and Fu-Sheng Yu, *Charm CPV: observation and prospects*, *Science Bulletin* **65** (2020) 1428. [arXiv:2002.12088]
- [9] F. Buccella, A. Paul and P. Santorelli, *$SU(3)_F$ breaking through final state interactions and CP asymmetries in $D \rightarrow PP$ decays*, *Phys. Rev. D* **99** (2019) 113001. [arXiv:1902.05564]
- [10] J. P. Alexander *et al.* [CLEO Collaboration], *Absolute measurement of hadronic branching fractions of the D_s^+ meson*, *Phys. Rev. Lett.* **100** (2008) 161804. [arXiv:0801.0680]
- [11] H. Mendez *et al.* [CLEO Collaboration], *Measurements of D meson decays to two pseudoscalar mesons*, *Phys. Rev. D* **81** (2010) 052013. [arXiv:0906.3198]
- [12] P. U. E. Onyisi *et al.* [CLEO Collaboration], *Improved measurement of absolute hadronic branching fractions of the D_s^+ meson*, *Phys. Rev. D* **88** (2013) 032009. [arXiv:1306.5363]

- [13] M. Ablikim *et al.* [BESIII Collaboration], *Measurement of the center-of-mass energies at BESIII via the di-muon process*, *Chin. Phys. C* **40** (2016) 063001. [arXiv:1510.08654]
- [14] M. Ablikim *et al.* [BESIII Collaboration], *Precision measurement of the integrated luminosity of the data taken by BESIII at center of mass energies between 3.810 GeV and 4.600 GeV*, *Chin. Phys. C* **39** (2015) 093001. [arXiv:1503.03408]
- [15] M. Ablikim *et al.* [BESIII Collaboration], *Design and construction of the BESIII detector*, *Nucl. Instrum. Meth. A* **614** (2010) 345. [arXiv:0911.4960]
- [16] C. Yu *et al.*, *BEPCII performance and beam dynamics studies on luminosity*, *JACoW-IPAC2016-TUYA01*.
- [17] X. Li *et al.*, *Study of MRPC technology for BESIII endcap-TOF upgrade*, *Radiat. Detect. Technol. Methods* **1** (2017) 13;
- [18] Y. X. Guo *et al.*, *The study of time calibration for upgraded end cap TOF of BESIII*, *Radiat. Detect. Technol. Methods* **1** (2017) 15.
- [19] S. Agostinelli *et al.* [GEANT4 Collaboration], *GEANT4: A Simulation toolkit*, *Nucl. Instrum. Meth. A* **506** (2003) 250.
- [20] S. Jadach, B. F. L. Ward and Z. Was, *Coherent exclusive exponentiation for precision Monte Carlo calculations*, *Nucl. Phys. B Proc. Suppl.* **89** (2000) 106; [arXiv:hep-ph/0012124]
- [21] *The precision Monte Carlo event generator KK for two-fermion final states in e^+e^- collisions*, *Comput. Phys. Commun.* **130** (2000) 260. [arXiv:hep-ph/9912214]
- [22] D. J. Lange, *The EvtGen particle decay simulation package*, *Nucl. Instrum. Meth. A* **462** (2001) 152;
- [23] R. G. Ping, *Event generators at BESIII*, *Chin. Phys. C* **32** (2008) 599.
- [24] J. C. Chen, G. S. Huang, X. R. Qi, D. H. Zhang and Y. S. Zhu, *Event generator for J/ψ and $\psi(2S)$ decay*, *Phys. Rev. D* **62** (2000) 034003;
- [25] R. L. Yang, R. G. Ping and H. Chen, *Tuning and validation of the lundcharm model with J/ψ decays*, *Chin. Phys. Lett.* **31** (2014) 061301.
- [26] E. Richter-Was, *QED bremsstrahlung in semileptonic B and leptonic τ decays*, *Phys. Lett. B* **303** (1993) 163.
- [27] R. G. Ping, *An exclusive event generator for e^+e^- scan experiments*, *Chin. Phys. C* **38** (2014) 083001. [arXiv:1309.3932]
- [28] M. Ablikim *et al.* [BESIII Collaboration], *Observation of $\chi_{cJ} \rightarrow 4K_S^0$* , *Phys. Rev. D* **99** (2019) 052008. [arXiv:1901.08207]
- [29] M. Ablikim *et al.* [BESIII Collaboration], *Preliminary value of $\mathcal{B}(D_s^+ \rightarrow a_1(1260)^+\eta) = 0.0670 \pm 0.0081$ is quoted, to be published.*
- [30] M. Ablikim *et al.* [BESIII Collaboration], *Study of the decays $D_s^+ \rightarrow K_S^0 K^+$ and $K_L^0 K^+$* , *Phys. Rev. D* **99** (2019) 112005. [arXiv:1903.04164]
- [31] M. Ablikim *et al.* [BESIII Collaboration], *Improved measurement of the absolute branching fraction of $D^+ \rightarrow \bar{K}^0 \mu^+ \nu_\mu$* , *Eur. Phys. J. C* **76** (2016) 369. [arXiv:1605.00068]
- [32] M. Ablikim *et al.* [BESIII Collaboration], *Measurement of the absolute branching fraction of $D^+ \rightarrow \bar{K}^0 e^+ \nu_e$ via $\bar{K}^0 \rightarrow \pi^0 \pi^0$* , *Chin. Phys. C* **40** (2016) 113001. [arXiv:1605.00208]

- [33] M. Ablikim *et al.* [BESIII Collaboration], *Study of decay dynamics and CP asymmetry in $D^+ \rightarrow K_L^0 e^+ \nu_e$ decay*, *Phys. Rev. D* **92** (2015) 112008. [arXiv:1510.00308]